Available online at www.sciencedirect.com

ScienceDirect

IFAC PapersOnLine 58-9 (2024) 241–246

Innovative Device for Measuring Energy-Harvesters

F. Rusnák * **J. Arm** ** **P. Fiedler** ***

* *Brno University of Technology, Department of control and instrumentation CZ (Tel: +420 605311719; e-mail: xrusna06@vutbr.cz)*

** *Brno University of Technology, Department of control and instrumentation CZ (Tel: +420 541146420; e-mail: arm@vut.cz)*

*** *Brno University of Technology, Department of control and instrumentation CZ (Tel: +420 541146480; e-mail: fiedlerp@vut.cz)*

Abstract: In recent years, the topic of Energy-Harvesters has been increasingly discussed. New materials are constantly being developed to make it more efficient to harvest energy from the environment, which can be collected in various forms. New materials and Energy-Harvesters are measured to verify their effectiveness and many are tested under practical conditions. Comprehensive measurements are needed to verify the theoretical designs, for which, among other measuring instruments, resistive loading is used. This paper presents the design and implementation of an optimized electronic resistive load, which allows the automation of measurements through communication using SCPI commands. Due to its compact size, it allows working even in field conditions.

Keywords: Energy Harvester, Resistor decade, Synthetics resistor, Micro power load, Innovation electrotechnics, Measurement micro-power sources

1. INTRODUCTION

With the rapid development of electronic devices and the improvement of their features, their size and weight are decreasing. However, this trend is not commensurate with the development of batteries, which are heavy, bulky and temperature sensitive compared to electronics. Their size and weight often dominate the electronic circuitry itself, and in addition their limited lifetime requires replacements, which can be a source of problems in, for example, bio-medical devices or sensor networks Sezer and Koç (2021).

For most systems operating under practical conditions, it is crucial to know their state, which is obtained by measurement. One use is to monitor temperature, vibration and machine noise. Early detection of wear and tear on mechanical machines Machine Condition Monitoring (MCM) and their maintenance reduces the risk of potential accidents and losses in the industry. The use of Wireless Sensor Nodes (WSN) automates the entire measurement process. When measuring on large-scale systems such as highways or railway lines, the use of wireless sensor nodes represents a significant savings on cabling Hodge et al. (2015). Furthermore, the use of wireless sensors is also suitable for shorter distances, for example in aircraft where weight is a critical parameter Ahmad et al. (2021), or in cars where tire pressure is measured Fu et al. (2021), where it would be impractical to implement a wired connection. According to Williams et al. (2021), energy can be harvested in various forms such as solar radiation, fluid flow, radio waves, magnetism, thermal elergy and mechanical vibration, some of which are of natural origin and others are human generated.

Piezo-elements are one of the common ways to harvest energy from the environment. According to Kim (2011), piezo materials are classified into two categories. Piezoceramic materials offering a high electro-mechanical coupling constants. However, they are very brittle. In contrast, piezopolymers are highly flexible, but they have a lower electro-mechanical coupling constants. There are two main phenomena, the direct piezo-electric effect described by equation 1 and the converse piezo-electric effect described by equation 2, which can be written in linearized form.

Direct piezoelectric effect:

$$D_i = e_{ij}^{\sigma} E_j + d_{im}^{d} \sigma_m \tag{1}$$

Converse piezoelectric effect:

$$\varepsilon_k = d_{jk}^{c} E_j + S_{km}^{E} \sigma_m \tag{2}$$

Where vector D_i is the dielectric displacement, ε_k is the strain vector, E_j is the applied electric field vector, and σ_m is the stress vector.

According to a comprehensive survey Sezer and Koç (2021), from 2000 to 2019, there has been an increasing number of documents dealing with Energy-Harvesting, amounting to 1172. Despite the increasing interest, effective methods for comprehensive measurement of PEHs are not applied. One aspect that may affect the development of PEHs across the board is the streamlining of the measurement and testing process itself, which currently appears to be lengthy and inefficient.

10.1016/j.ifacol.2024.07.403

1.1 Application of resistor decades

The measurement system includes an excitation Energy-Harvester, voltmeter, or oscilloscope for detailed signal analysis. The schematic in Figure 1 shows the principle measurement PEH, which uses a connected variable resistive load to simulate the draw of the powered device.

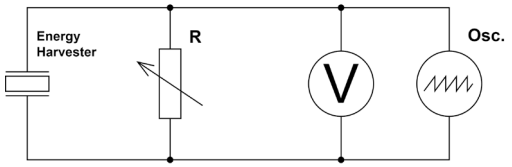

Fig. 1. Principle wiring diagram of the PEH measuring system

Variable resistance R is used to achieve maximum efficiency. The design of the optimal resistive load is discussed in Yang et al. (2017) and Kunz et al. (2021) compares the theoretical design of resistive load and frequency with complex measured data.

Measurement circuit with a manual resistive decade, such as Zhang et al. (2024), does not allow automation of the measurement and operation of such a decade can be tedious and impractical. Furthermore, the proposal Xia et al. (2024) uses a fixture with resistors that would be difficult to use for measurements under practical conditions. The main limitation imposed by the use of manual resistive decads is the time consuming and tedious measurements required to smoothly plot the characteristics in graphs.

The connection of manual resistive loads is mentioned in a wide range of literature dealing with Energy-Harvesters. For example, Ahmad et al. (2023), Costa and Savi (2024) and Wei et al. (2023) mention the connection of ballast loads, but do not further elaborate on their effective use in measurements. Facilitating field measurements such as Cámara-Molina et al. (2024) would be possible using a small portable resistive load device that is easy to operate. This could result in easier acquisition of more valuable data even under conditions where this would not otherwise be possible.

The current state of the market does not provide many optimal resistive load solutions for measuring PEHs. For example, although the device described in Pavliska (2017) is an accurate laboratory device that is adjustable via serial communication, it exhibits low accuracy for dynamic signals at high generated resistance. The device is not suitable for carrying because it is bulky and impractical for field use.

Automating the process of setting the value of the optimized resistive decade has the potential to simplify the measurement process for the user, significantly reduce measurement time, and enable the acquisition of more detailed data. The basic premise is an easily user-adjustable resistive decade with no non-negligible parasitic parameters affecting the measured parameters.

2. MEASUREMENT SURVEY

In order to optimize the new design of the resistive decade, it is difficult to know the conditions in which the device will occur, according to which its parameters can be specified. The key parameters of a resistive load are the maximum voltage, current, power and range of resistance generated. Last but not least, it is also necessary to know the frequency range. The requirements for the resistive load parameters were designed based on a survey of measurement parameters.

In the case of measurements Ahmad et al. (2021), powers up to 100μW were obtained. The frequency ranges from 50Hz to 130Hz, but the acoustic energy collection takes place at resonant frequencies up to 4.92kHz. The magnetostrictive harvester as proposed by Wei et al. (2023) can increase the efficiency of the signal and amplify its levels to voltage values of 1356mV and power of 26.2mW at a resonant frequency of 45Hz. By using the Adaptive Kinetic Energy Rellocation (AKER) mechanism described by Xia et al. (2024), energy can be harvested even at low frequencies around 1.2Hz. By tuning the resonant frequency of the harvester to the frequency of the source, further efficiency gains can be achieved such as Cámara-Molina et al. (2024) where frequencies ranged from 4.9Hz to 9.3Hz. Significant frequency components in the railroad bridge measurements were below the 30Hz threshold. The resonant frequencies can be in the lower kilo-Hertz orders as described in Zhao et al. (2011). The generated signals can also contain several resonant frequencies as in the vortex shedding-induced vibration described in Hu et al. (2018) where resonant frequencies of 9.89, 60.01 and 324.82Hz are recorded. DC-DC boost converters are often used for effective voltage conversion at the PEH terminals, where Kim (2011) reports functionality at 572Hz.

The paper Lin et al. (2021) gives a broad overview of different energy harvesting principles, where the resonant frequencies range from 33Hz to 10155Hz. A detailed overview of PEHs is provided by Sezer and Koç (2021). The most commonly measured voltages range up to 30V. In some cases, higher voltages around 60V are recorded and the highest voltages can be up to 112V. The currents of the piezo elements vary by several orders of magnitude as well. The currents are lower than 12.2μA. Occasionally, currents as high as 1.45mA are recorded. The estimation of the frequency parameters of the harvesters is not mentioned too much. The numerical values are below 100Hz. In many cases, harvester-human interactions are mentioned, such as the touch of a finger, the movement of a human knuckle, or the slamming of a fist. Assuming that energy is harvested from the movement of human joints, the effective frequency range according to Meng et al. (2006) is less than 10Hz.

2.1 Summary the parameters of measurements

The above survey of measurement methods and parameters of Energy-Harvesters indicates the frequent use of manual resistance decads. However, the methods used may not always be completely efficient and the instruments used do not allow for automation of the measurements. Below is a solution that can help to make the testing and measurement of Energy-Harvesters more efficient and faster. The solution is a new design of an optimized resistive load that is compatible with the parameters of most Energy-Harvesters. An important functionality is the

serial communication, which will allow remote parameter setting and thus automation of measurements. In addition, the optimization of the instrument will lead to a reduction in size. A compact device that can also be deployed in field conditions is desirable.

Based on a survey of common electrical parameters of Energy-Harvesters, upper limits of 112V voltage, 1.45mA or $670nA \cdot cm^{-2}$ current, 0.98mW or $9.3mW \cdot cm^{-3}$ power, and frequency ranges up to 10kHz were found. Most PEHs, however, exhibit much lower values. Considering the available hardware resources and the most common parameter values of PEHs, the resistive decade requirements have been determined: 40V, 2mA and 350Hz.

3. ACTIVE GENERATOR OF SYNTHETICS RESISTANCE

In order to adapt the device to the requirements of the application, it was necessary to fundamentally rethink its entire design. The spatially expressive resistor matrix circuitry was replaced by a new design that uses semiconductor components to generate a synthetic resistance R_S. The internal circuit in Figure 2 uses only three operational amplifiers. The generated resistance depends on two controllable parameters. The switchable resistors R provide coarse adjustment of the generated resistance R_S. The fine step of the desired R_S is provided by the adjustable gain of the Au operational amplifier. The circuitry is powered by a galvanically isolated symmetrical DC-DC power supply. The operational amplifiers are supplied with a voltage of $\pm 20V$ from which the maximum voltage at the input terminals is derived. A second $\pm 2.5V$ supply voltage circuit supplies the electronic potentiometer. The entire circuit is controlled by an STM32F303 microprocessor, which provides communication with the higher-level system.

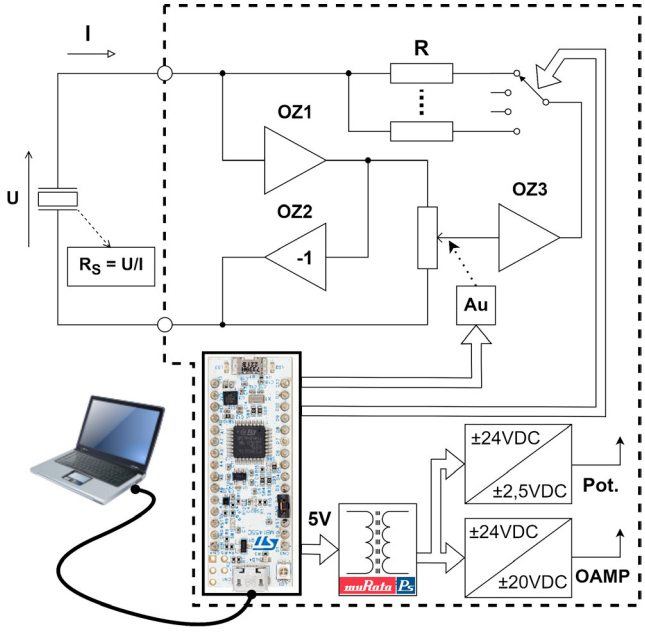

Fig. 2. Block diagram of the device

The principle of generating a synthetic resistor is based on a forced voltage change on the physical resistor. The resulting voltage on the resistor, which is shown in Figure 3, is formed by the difference between the input voltage U and the controlled voltage U_D.

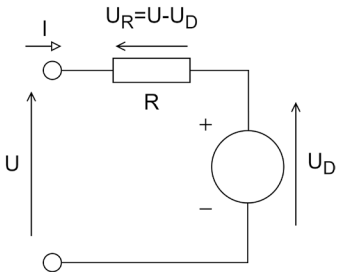

Fig. 3. Basics principle of synthetic resistance

By controlling the voltage U_D the current flowing through the resistor R is affected according to the equation 3.

$$I = \frac{U - U_D}{R} = \frac{U - A_u U}{R} = \frac{U\,(1 - A_u)}{R} \tag{3}$$

By changing the gain of A_u, the current through the resistor R is affected and the apparent resistance Rs can be adjusted, which is expressed by the equation 4 for an asymmetrically powered circuit.

$$R_S = \frac{U}{\frac{U - A_u U}{R}} \Rightarrow R_S = \frac{R}{1 - A_u} \tag{4}$$

3.1 Maximum voltage swing

The maximum voltage at the terminals of the Energy-Harvester is limited by the magnitude of the supply voltage of the operational amplifiers. Due to the AC voltage generated, the electronics must be powered symmetrically. A simple and common solution in electronic circuit designs is to connect one terminal to zero potential. However, such a connection only allows an amplitude half that of the full potential of the power supply levels.

The design shown in Figure 2 is capable of handling amplitudes that span the entire supply voltage range, thanks to the active Driving Around Zero (DAZ) control provided by the OZ2 operational amplifier. The voltage levels at the input terminals are symmetrical with respect to each other, allowing the voltage at the input terminals to reach up to ±40V without damaging sensitive electronics.

The design of the internal electronics is carried out for voltage levels that are considered relative to the centre zero voltage. In DAZ, the equation 4 must be modified to the form 5 to calculate the generated resistance.

$$R_S = \frac{2R}{1 - A_u} \tag{5}$$

Due to the inverted voltage generated by the DAZ, it is also possible to realize a negative gain of A_u, thus increasing the range of the generated resistance R_S.

3.2 Gain adjustment

Due to hardware limitations, the gain of the operational amplifier A_u in Figure 2 may be in the range $\langle -1, 1 \rangle$. The relationship between the values of R_S and A_u described by equation 5 is strongly nonlinear and does not provide a suitable characterization of R_S. A suitable resistive ballast

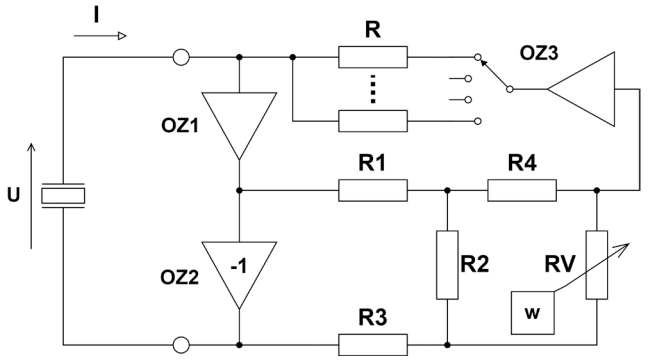

Fig. 4. Linearization circuit diagram

characteristic is characterized by a constant relative step. The problem is solved using the optimized circuit of the resistor array and electronic rheostat in Figure 4. Resistors R1, R2, R3 act as voltage divider, and reduce the signal magnitude due to the $\pm 2.5V$ supply range of the electronic rheostat. The signal is again amplified by OZ3, which provides a gain of 10.

The total optimized gain of the A_u signal depending on the position of the slider w is expressed by the equation 6, where R_i is the internal resistance of the system, d is the number of rheostat bits and RV is the rheostat value.

$$A_u = 10 * \left(\frac{R3}{R_i} - \frac{RVw\left(\frac{R1+R3}{R_i} - 1\right)}{R4\left(2^d - 1\right)RVw} - \frac{1}{2} \right) \tag{6}$$

The equation 7 expresses the internal resistance of the resistive circuit with electronic rheostat RV.

$$R_i = R1 + R3 + \frac{1}{\frac{1}{R2} + \frac{1}{\frac{RVw}{2^d-1} + R4}} \tag{7}$$

The resulting generated resistance is obtained by substituting 6 into 5, where R is the current value of the switchable resistance.

The output waveforms can be compared on the Figure 5, where the non-uniformity of the relative step R_S, which is controlled by the linear waveform A_u, is evident. In contrast, the optimized circuit provides a fairly uniform relative step, which then appears as a nearly flat curve in the 6 plot with the logarithmic y-axis.

3.3 Electronics of active principle and parasitic properties

The described parasitic characteristics of operational amplifiers in Doleček (2007) are limited frequency response, CMRR, PMRR, noise at input terminals, noise at output terminals, voltage offset, current offset at input terminals, current to input terminals, parasitic capacitance at input terminals, output impedance, limited output terminal current, output edge slope, delay time, temperature dependence, limited operating temperature, quiescent supply current and limited supply voltage range. The highest error is caused by current leakage from the operational amplifier input terminals and offset voltage. These errors manifest themselves as nonlinear characteristics of the resistive load. It can be observed in the Figure 7 that the error increases dramatically as A_u approaches the value of 1

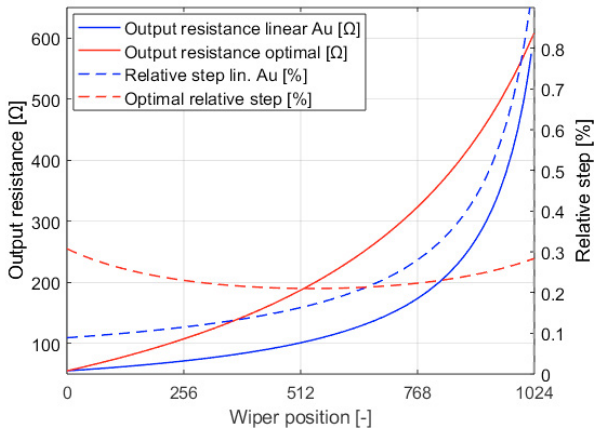

Fig. 5. Comparison of Generated Output Resistance Characteristics

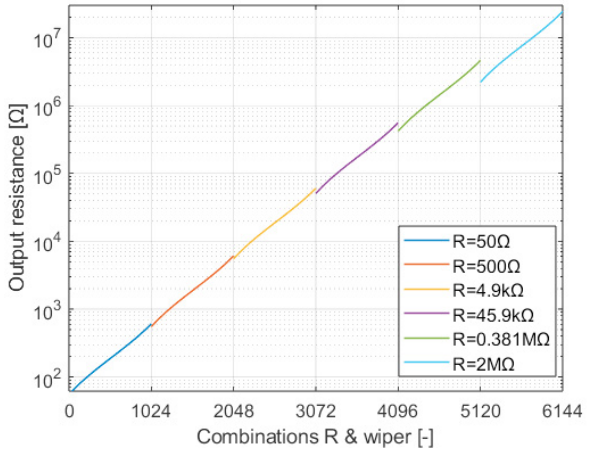

Fig. 6. Characteristics of the generated resistance over the whole range

and is most pronounced at the low voltage generated by PEH. The values in the Figure 7 are for the relative error caused by the offset voltage of the operational amplifiers for a temperature range of 40C°.

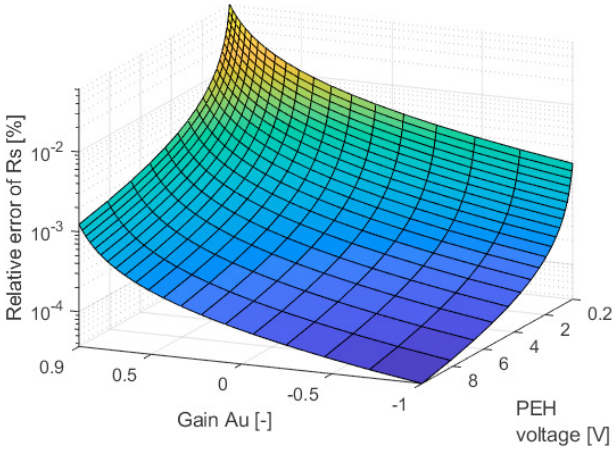

Fig. 7. Relative error of generated resistance caused by OZ offset voltages

Non-zero input terminal current has a similar effect. The leakage current causes a voltage drop across the internal resistance of PEH. Therefore, an operational amplifier, serving as a buffer, with a very small leakage current of a few tens of pA and a low offset voltage of a few μV is connected to the input terminals.

4. APPLICATION OF HARDWARE

Based on the proposed electrical circuit principles, the Printed Circuit Board (PCB) was designed and the device shown in Figure 8 was assembled. The device allows communication with a computer via a serial link. Only five mechanical relays are switched, but the step of the required resistance is fine due to the active circuits that generate the synthetic resistance. The resistive decade circuits themselves are galvanically isolated from the digital circuits. The resistive decade is therefore floating. Another advantage of the device is the voltage tracker, which allows the measurement of the voltage waveform on the Energy-Harvester without the impedance of the measuring device affecting the measurement.

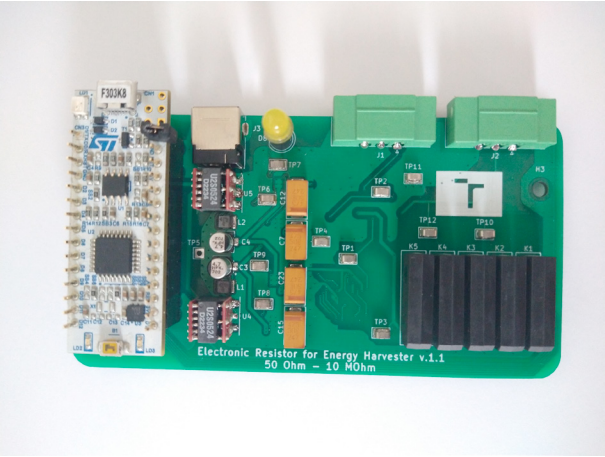

Fig. 8. PCB of device

For the DC signal, the accuracy of the resistive decade was measured to be below 1% for the entire range of adjustable resistance shown in Figure 9.

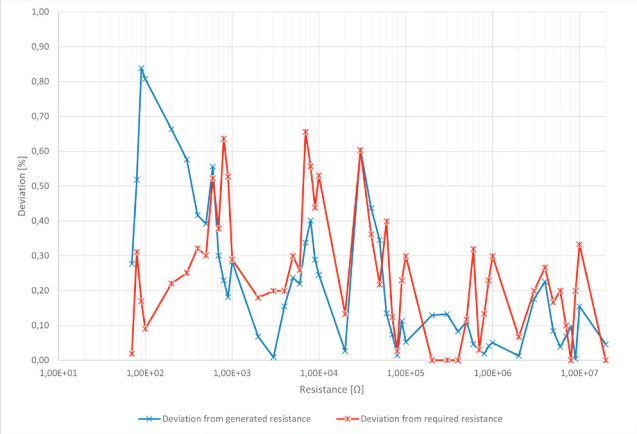

Fig. 9. Static characteristic of device

The characteristic for the dynamic signal is plotted in the Figure 10. The device is capable of generating resistance with sub 1% accuracy for frequencies up to 2.5kHz for a set resistance up to 300$k\Omega$. Neglecting the dip in the curve at the 470$k\Omega$ setpoint, the device can be said to exhibit 1% accuracy up to a set generated resistance of up to 3$M\Omega$ for a 1kHz signal.

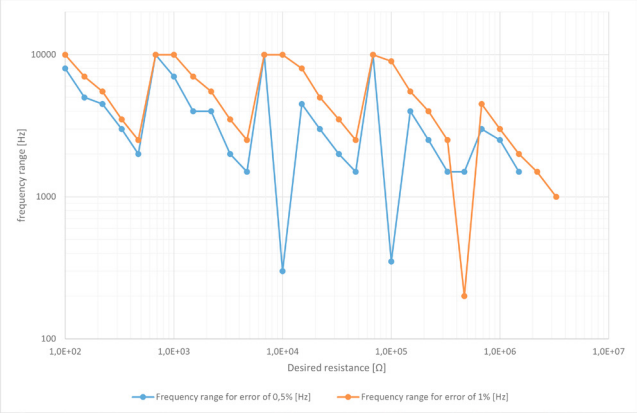

Fig. 10. Dynamic characteristic of device

5. CONCLUSION

Energy-Harvesters have been an increasingly discussed topic in recent years. However, their measurement and testing under field conditions is inefficient and time-consuming due to the use of outdated instruments. The proposal focuses on streamlining electronic resistive decade devices. The required device parameters were defined through a survey of articles dealing with the issue.

To make the device circuitry more efficient, the principle of synthetic resistance generation was used, which is based on an analog circuit with operational amplifiers. The result is a small compact resistive decade device that provides a range of values from 70Ω to 20$M\Omega$ with 1% accuracy. The device maintains 1% accuracy at a dynamic signal of 2.5kHz up to a setpoint of the desired resistance of 300$k\Omega$. With a voltage buffer used for impedance decoupling, measurements can be made without the wiring being affected by the parasitic characteristics of the measuring instruments. Another feature is the control of the resistive decade using SCPI commands. Serial line control streamlines the measurement process and enables automation of complex and lengthy measurements.

REFERENCES

Ahmad, I., Hee, L.M., Abdelrhman, A.M., Imam, S.A., and Leong, M. (2021). Scopes, challenges and approaches of energy harvesting for wireless sensor nodes in machine condition monitoring systems: A review. *Measurement*, 183, 109856. doi: https://doi.org/10.1016/j.measurement.2021.109856. URL `https://www.sciencedirect.com/science/article/pii/S0263224121008009`.

Ahmad, I., Tosif, A., Abdelrhman, A.M., Chithambaram, S., Imam, S.A., and Hammad, M. (2023). Design development and testing of traffic induced wind based artificial tree type hybrid energy harvester for wireless sensor nodes. *Results in Engineering*, 20, 101515. doi:https://doi.org/10.1016/j.rineng.

2023.101515. URL https://www.sciencedirect.com/science/article/pii/S2590123023006424.

Cámara-Molina, J., Romero, A., Moliner, E., Connolly, D., Martínez-Rodrigo, M., Yurchenko, D., and Galvín, P. (2024). Design, tuning and in-field validation of energy harvesters for railway bridges. *Mechanical Systems and Signal Processing*, 208, 111012. doi:https://doi.org/10.1016/j.ymssp.2023.111012. URL https://www.sciencedirect.com/science/article/pii/S0888327023009202.

Costa, L.G. and Savi, M.A. (2024). Nonlinear dynamics of a compact and multistable mechanical energy harvester. *International Journal of Mechanical Sciences*, 262, 108731. doi:https://doi.org/10.1016/j.ijmecsci.2023.108731. URL https://www.sciencedirect.com/science/article/pii/S0020740323006331.

Doleček, J. (2007). *Moderní učebnice elektroniky*. BEN - technická literatura, Praha, 1. edition.

Fu, H., Mei, X., Yurchenko, D., Zhou, S., Theodossiades, S., Nakano, K., and Yeatman, E.M. (2021). Rotational energy harvesting for self-powered sensing. *Joule*, 5(5), 1074–1118. doi:https://doi.org/10.1016/j.joule.2021.03.006. URL https://www.sciencedirect.com/science/article/pii/S254243512100101X.

Hodge, V.J., O'Keefe, S., Weeks, M., and Moulds, A. (2015). Wireless sensor networks for condition monitoring in the railway industry: A survey. *IEEE Transactions on Intelligent Transportation Systems*, 16(3), 1088–1106. doi:10.1109/TITS.2014.2366512.

Hu, Y., Yang, B., Chen, X., Wang, X., and Liu, J. (2018). Modeling and experimental study of a piezoelectric energy harvester from vortex shedding-induced vibration. *Energy Conversion and Management*, 162, 145–158. doi:https://doi.org/10.1016/j.enconman.2018.02.026. URL https://www.sciencedirect.com/science/article/pii/S0196890418301304.

Kim, Heung Soo, K.J.H.K.J. (2011). A review of piezoelectric energy harvesting based on vibration. *International Journal of Precision Engineering and Manufacturing*, 12. URL https://doi.org/10.1007/s12541-011-0151-3.

Kunz, J., Fialka, J., Pikula, S., Benes, P., Krejci, J., Klusacek, S., and Havranek, Z. (2021). A new method to perform direct efficiency measurement and power flow analysis in vibration energy harvesters. *Sensors*, 21(7). doi:10.3390/s21072388. URL https://www.mdpi.com/1424-8220/21/7/2388.

Lin, Y.C., Tseng, K.S., and Ma, C.C. (2021). Investigation of resonant and energy harvesting characteristics of piezoelectric fiber composite bimorphs. *Materials and Design*, 197, 109267. doi:https://doi.org/10.1016/j.matdes.2020.109267. URL https://www.sciencedirect.com/science/article/pii/S0264127520308029.

Meng, Q., Li, B., and Holstein, H. (2006). Recognition of human periodic movements from unstructured information using a motion-based frequency domain approach. *Image and Vision Computing*, 24(8), 795–809. doi:https://doi.org/10.1016/j.imavis.2006.01.033. URL https://www.sciencedirect.com/science/article/pii/S0262885606000874.

Pavliska, V. (2017). Programovatelná odporová dekáda. URL https://www.vut.cz/www_base/zav_prace_soubor_verejne.php?file_id=147917.

Sezer, N. and Koç, M. (2021). A comprehensive review on the state-of-the-art of piezoelectric energy harvesting. *Nano Energy*, 80, 105567. doi:https://doi.org/10.1016/j.nanoen.2020.105567. URL https://www.sciencedirect.com/science/article/pii/S2211285520311411.

Wei, L., Liu, H., Shu, L., Zhao, L., Liu, Z., and Chang, Y. (2023). Study of a magnetostrictive energy harvester for harvesting transient shock vibration. *Sensors and Actuators A: Physical*, 361, 114577. doi:https://doi.org/10.1016/j.sna.2023.114577. URL https://www.sciencedirect.com/science/article/pii/S0924424723004260.

Williams, A.J., Torquato, M.F., Cameron, I.M., Fahmy, A.A., and Sienz, J. (2021). Survey of energy harvesting technologies for wireless sensor networks. *IEEE Access*, 9, 77493–77510. doi:10.1109/ACCESS.2021.3083697.

Xia, G., Lu, Q., Cai, M., Li, X., Zhang, D., Wang, C., and Liao, W.H. (2024). Comprehensive investigation of a broadband wearable energy harvester using adaptive kinetic energy reallocation mechanism. *Mechanical Systems and Signal Processing*, 206, 110907. doi:https://doi.org/10.1016/j.ymssp.2023.110907. URL https://www.sciencedirect.com/science/article/pii/S0888327023008154.

Yang, Z., Erturk, A., and Zu, J. (2017). On the efficiency of piezoelectric energy harvesters. *Extreme Mechanics Letters*, 15, 26–37. doi:https://doi.org/10.1016/j.eml.2017.05.002. URL https://www.sciencedirect.com/science/article/pii/S2352431617300482.

Zhang, L., Kan, J., Lin, S., Liao, W., Yang, J., Liu, P., Wang, S., and Zhang, Z. (2024). Design and performance evaluation of a pendulous piezoelectric rotational energy harvester through magnetic plucking of a fan-shaped hanging composite plate. *Renewable Energy*, 222, 119796. doi:https://doi.org/10.1016/j.renene.2023.119796. URL https://www.sciencedirect.com/science/article/pii/S0960148123017111.

Zhao, Z., Li, Y., Chen, J., and Xu, J. (2011). Grain separation loss monitoring system in combine harvester. *Computers and Electronics in Agriculture*, 76(2), 183–188. doi:https://doi.org/10.1016/j.compag.2011.01.016. URL https://www.sciencedirect.com/science/article/pii/S0168169911000354.

ACKNOWLEDGEMENTS

This research was supported by the grants "Research in Automation, Cybernetics and Artificial Intelligence within Industry 4.0" financially supported by the Internal science fund of Brno University of Technology, grant number FEKT-S-20-62